Impairments in sensory-motor gating and information processing in a mouse model of *Ehmt1* haploinsufficiency

Brittany A. Davis[1], François David[1], Ciara O'Regan[2], Manal A. Adam[2], Adrian J. Harwood[1], Vincenzo Crunelli[1] & Anthony R. Isles[2#]*

[1]Neuroscience and Mental Health Research Institute and School of Biosciences, Cardiff University, Cardiff, UK

[2]MRC Centre for Neuropsychiatric Genetics and Genomics, School of Medicine, Cardiff University Cardiff, UK

*Correspondence to: Anthony Isles, MRC CNGG, Cardiff University, Hadyn Ellis Building, Maindy Road, Cardiff, CF24 4HQ, UK; Email: *IslesAR1@cardiff.ac.uk*; Tel. ++44(0)2920688467

ABSTRACT

Regulators of chromatin dynamics and transcription are increasingly implicated in the aetiology of neurodevelopmental disorders (NDDs). Haploinsufficiency of *EHMT1*, encoding a histone methyl-transferase, is associated with several NDDs, including Kleefstra syndrome, developmental delay and autism spectrum disorder. Using a mouse model of *Ehmt1* haploinsufficiency (*Ehmt1*$^{D6Cre/+}$), we examined a number of brain and behavioural endophenotypes of relevance to NDDs. Specifically, we show that *Ehmt1*$^{D6Cre/+}$ mice have deficits in information processing, evidenced by abnormal sensory-motor gating, a complete absence of object recognition memory and a reduced magnitude of auditory evoked potentials in both paired-pulse inhibition and mismatch negativity (MMN). The electrophysiological experiments show that differences in magnitude response to auditory stimulus were associated with marked reductions in total and evoked beta- and gamma-band oscillatory activity, as well as significant reductions in phase synchronisation. The pattern of electrophysiological deficits in *Ehmt1*$^{D6Cre/+}$ matches those seen in control mice following administration of the selective NMDA antagonist, ketamine. This, coupled with reduction of *Grin1* mRNA expression in *Ehmt1*$^{D6Cre/+}$ hippocampus, suggests that *Ehmt1* haploinsufficiency may lead to disruption in NMDA-R. Taken together, these data indicate that reduced *Ehmt1* dosage during forebrain development leads to abnormal circuitry formation, which in turn results in profound information processing deficits. Such information processing deficits are likely paramount to our understanding of the cognitive and neurological dysfunctions shared across the NDDs associated with *EHMT1* haploinsufficiency.

Keywords: Neurodevelopmental disorders; mouse model; startle and PPI; auditory event related potentials; NMDA-R hypofunction

INTRODUCTION

Post-translational modifiers of histone proteins influence chromatin dynamics and transcriptional regulation throughout development and are essential for the highly choreographed processes of lineage commitment and differentiation during neurodevelopment [1, 2]. Perhaps unsurprisingly, exome sequencing studies and pathway analyses of genome wide association studies implicate genes encoding chromatin and transcriptional regulators in the aetiology of autism spectrum disorders [3, 4], schizophrenia [5] and severe developmental disorders [6, 7]. One such gene, implicated in several neurodevelopmental and neuropsychiatric disorders [8], is *EHMT1,* which encodes the histone H3 lysine 9 mono- and di-methyltransferase G9a-like protein (GLP).

Haploinsufficiency of *EHMT1* is the primary cause of the 9q34 subtelomeric-deletion syndrome, also known as Kleefstra Syndrome [9, 10], a condition associated with intellectual disabilities, epilepsy, childhood hypotonia, facial dysmorphism, microcephaly, delays in reaching developmental milestones and behavioural problems such as aggressive outbursts and hypoactivity. Furthermore, analysis of Copy Number Variants (CNVs) [11] and a large exome sequencing study [7] have linked *de novo* mutations affecting *EHMT1* to severe developmental delay more generally. Finally, CNVs spanning *EHMT1* have also been associated with autism spectrum disorder [12] and schizophrenia [13]. The severity and breadth of neurodevelopmental and neuropsychiatric phenotypes associated with changes in *EHMT1* dosage are a strong indication of the central importance of this gene to brain development and function [8]. This is supported by data from animal models that demonstrate a range of brain and behavior deficits reminiscent of neurodevelopmental disorders including anxiety phenotypes [14], contextual fear memory [15, 16], and synaptic scaling [17].

Here we explore endophenotypes of relevance to psychiatric problems seen in those carrying mutation of *EHMT1*, using a mouse model of *Ehmt1* haploinsufficiency (*Ehmt1*$^{D6Cre/+}$ mice). Specifically, we find deficits in sensory motor-gating and novel object recognition. A reduction in the magnitude of auditory evoked potentials in paired-pulse inhibition and MMN, provides electrophysiological evidence of an impairment in information processing in the *Ehmt1*$^{D6Cre/+}$ mice. Gene expression data and pharmacological manipulation are suggestive of NMDA-R

hypofunction in *Ehmt1*$^{D6Cre/+}$ adult mouse contributing to the sensory-motor gating and information processing deficits.

MATERIALS AND METHODS

Animals

All procedures were conducted in accordance with the requirements of the UK Animals (Scientific Procedures) Act 1986, with additional ethical approval at Cardiff University.

In order to generate experimental cohorts, *Ehmt1*$^{fl/fl}$ [18] male studs were paired in trios with one homozygous females carrying two copies of the Tg(Dach1-cre)1Krs/Kctt Cre transgene, maintained on a F1(C57BL/6J x CBA/Ca) background; and one wild-type F1(C57BL/6J x CBA/Ca) female. Experimental cohorts were reared together and then weaned into mixed cages (2-5per cage) of *Ehmt1*$^{D6cre/+}$ (experimental line) and *Ehmt1*$^{fl/+}$ mice (control line) (see Supplementary Figure 2). All experimental subjects were male mice, and aged between 4-8 months during testing. Animals were housed 12 hour light/12 hour dark (lights on at 7am), and standard laboratory diet and water were available *ad libitum* throughout testing. Experimenters were blind to the genotype of animals during behavioural testing.

Behaviour

All animals were initially subject to sensory-motor gating testing (*Ehmt1*$^{fl/+}$, n=25; *Ehmt1*$^{D6cre/+}$ mice, n=31). A subset of these were then tested on the rotor-rod (*Ehmt1*$^{fl/+}$, n=9; *Ehmt1*$^{D6cre/+}$ mice, n=18) and the remainder on the novel object recognition memory test (*Ehmt1*$^{fl/+}$ mice, n=16; *Ehmt1*$^{D6cre/+}$ mice, n=13).

Sensory-motor gating

Acoustic startle response (ASR) and prepulse inhibition (PPI) of the startle response were monitored using a SR-Lab apparatus (San Diego Instruments, U.S.A) modified for use in mice, according to published methods [19]. Briefly, animals were placed in a Perspex tube (internal diameter 35mm) and white noise stimuli were presented via a speaker. The amount of movement relayed as their startle response was measured as a piezoelectric measure converted to arbitrary startle units. The measurement used was the maximum startle (Vmax). Due to the effect of weight on this reflex movement measurement, all data was normalised for individual body

weight. Pulse-alone trials consisted of a 40ms 120dB startle stimulus and a prepulse trial consisted of a 20ms prepulse at 4, 8, or 16db above background and a 40ms 120db startle stimulus, 70ms after the prepulse. The stimuli were presented in a pseudorandom manner every 15s. Whole body startle responses were recorded as the average startle during a 65ms window timed from the onset of the startle pulse.

Percentage PPI score for each trial was calculated:

[%PPI=100 × (ASRstartle pulse alone − ASRprepulse + startle pulse)/ASRstartle pulse alone].

Rotarod testing

A rotarod task (Ugo Basile, Italy) was used to assess motor learning and co-ordination. This consisted of a rotating rod 30 mm in diameter, with five separated chambers 57 mm in width, with a rod elevation of 160 mm. Motor learning was assessed across six rotarod sessions, one morning session and one evening session, on three consecutive days. The rod speed accelerated incrementally from 5-50rpm across the 300sec session. The main measure during training was latency to first fall. However, if the mice fell, they were continuously replaced on the rotating rod, until the full 300sec-session was over in order to prevent any confounds from arising from overall differences in time spent on the rotarod across sessions. In a separate test session on day four, the mice were given one 300-sec session at 10rpm, 20rpm, 30rpm, 40rpm and 50rpm consecutively in one morning session in order to assess motor coordination. Again the latency to first fall was recorded for each animal at each speed.

Novel object recognition memory

The NOR test arena was a square 30cm x 30cm with 30cm high, white Perspex walls. Four different, non-displaceable objects were used. All objects were white and selected for their equal appeal and available in triplicate to avoid the use of olfactory cues. In the habituation phase, 24hr prior to the task, each subject was allowed to explore the arena for 10min in the absence of objects. In the acquisition phase, the subject was returned to the arena containing 2 identical sample objects (A, A') and given 10min to explore. After a retention phase, consisting of 15min or 90min, the subject was returned to the arena with two objects, one identical to the sample and the other novel (A, B). During both the familiarization and test phase, objects were located adjacent corners of the arena. The location of the novel object was counterbalanced. To prevent

coercion to explore the objects, the subject was released in a third corner. Objects were cleaned with 70% ethanol wipes between sessions and object selection was randomized.

The main measure used was the Recognition Index (RI), indicating whether the animal investigated the novel object more than chance. This was calculated by the percentage of time spent investigating the novel object relative to the total object investigation [$RI= T_N/(T_N+T_F) \times 100$]. An RI significantly above chance or 50% indicates recognition of novelty and an RI equal to or below 50% indicates either no preference for the novelty or no recognition of novelty. Other parameters recorded were:overall time spent with each object, and frequency of visits to the zones containing an object. Data was collected in 1-min time bins across the 10-min session by a camera linked to a computer with Ethovision Observer software (Noldus, Nottingham, UK).

Electrophysiology

Adult male *Ehmt1*$^{D6Cre/+}$ mice (*n*=7) and *Ehmt1*$^{fl/+}$ control cage-mates (*n*=7) at 6-7 months of age were anesthetized with 2% isoflurane for stereotaxic electrode implantation. The electrode configuration used two bilateral frontal electrodes, one monopolar and one bipolar (2.7-mm anterior, 1.5-mm lateral, 1.2-deep relative to bregma); two bilateral hippocampal electrodes, one monopolar and one bipolar (2.7 mm posterior, 3-mm lateral, 2.2-mm deep relative to bregma); and one bipolar electrode in the auditory cortex (2.7-mm posterior, 4-mm lateral, 1.1-deep relative to bregma) as has been previously reported [20, 21] (for further details see Supplementary Materials and Methods, and Supplementary Figure 2). Due to animal loss, a subset of these was used in the MMN study; *Ehmt1*$^{D6Cre/+}$ mice (*n*=5) and *Ehmt1*$^{fl/+}$ control cage-mates (*n*=5).

ERPs were obtained by averaging EEG traces centred at time 0 and 500msec to 0μV, respectively. For each trial, power was calculated by using a complex Morlet's wavelets w(t, f0) [22]. The script used can be found at https://www.physics.lancs.ac.uk/research/nbmphysics/diats/tfr/. The wavelets have a Gaussian shape in the time domain (SD σt) and in the frequency domain (SD σt) around its central frequency *f*0: $w(t, f0)=A * \exp(-t2/2\ \sigma t2) * \exp(2i\pi f0t)$ with $\sigma f=1/\pi\sigma t$. The wavelet family we used was defined by $f0/\sigma f=1$, with f0 ranging from 0.5 to 100Hz in logarithmically distributed frequency steps (for full details see Supplementary Materials and Methods).

Auditory stimuli were generated using Spike2, version 7.2 and a Power1401 interface (CED, UK). Auditory stimulus was delivered with speakers positioned directly in front of each recording cage. Each mouse received an auditory, paired-pulse session and two sessions of mismatch negativity (MMN).

Paired pulse

Following Halene *et al*. [23], each mouse received an auditory, paired-pulse session in which a single tone was presented at 1500Hz and 90dB (S1) followed by a 500ms intra-trial interval and a second tone at 1500Hz and 90dB (S2). The tones were sinusoidal and 10ms in duration. The inter-pulse interval between the two tones was 10-s. Each mouse received 1250 paired-pulse trials per recording session.

Mismatch negativity

The mice also received two sessions of the MMN protocol. Similar to Ehrlichman *et al*. [20], the mice received 24 'standard' tones at 90dB and 1500Hz and one 'deviant' tone at 90dB and 2000Hz. All tones were sinusoidal and 10ms in duration and the intra-pulse interval between the 25 tones was 500-ms, while the inter-trial interval was 5-s. Each mouse was recorded for 360 trials in each of two sessions. In one session 10mg/kg of Ketamine was administered and in the second session an equal volume of saline was administered. The dosage of ketamine was chosen based on previous work [20, 21]. The within group design was counterbalanced by genotype and the order in which ketamine or saline sessions were administered. All recordings took place 5-mins after intraperitoneal injections of either 10mg/kg ketamine or the volume equivalent dose of saline. The waveform channels were filtered between 1 and 500Hz.

Gene Expression

RNA was extracted from macrodissected hippocampi using the RNeasy micro kit (Qiagen) following the manufacturers instructions. A 96 well RT^2 Custom Profiler PCR Array (CAPM12608, Qiagen) for mice was used. The custom genes list was generated based on GLP targets identified in the literature and tissue-specific relevance. For the qPCR array 1µg of total RNA was used and manufacture's instructions were followed, for cDNA synthesis—RT^2 First Strand Kit (Qiagen) and for the RT-PCR reaction—RT^2 SYBR Green ROX qPCR Matermix (Qiagen). The average Ct values across the three housekeeping genes *B2m, B-actin* and *Gapdh* were used as endogenous controls. ΔCt values were generated by normalizing to the geometric

mean of the Ct values for these three housekeeping genes. All individual reactions were carried out in triplicate. Real time qPCR data was visualized using the ΔΔCt method [24].

Statistics

All data were analyzed using SPSS 20 (SPSS, USA). The statistical differences between groups were analysed using independent samples t-tests, ANOVAs, or where appropriate Repeated Measures ANOVA (RP-ANOVAs). The main between-subject factor was GENOTYPE (*Ehmt1*$^{fl/+}$ controls or *Ehmt1*$^{D6Cre/+}$). The following within-subject factors were also analysed: TRIAL (Startle trial); PREPULSE (4, 8 or 16dB); SESSION and SPEED (rotarod); PULSE (standard or deviant in the MMN). To check for normal distribution, Mauchly's test of sphericity of the covariance matrix or Levenes test for equality of variances were applied. The more conservative Huynh-Feldt corrections, with adjusted degrees of freedom are reported in cases in which test assumptions were violated. Non-parametric analyses were as follows. For the NOR task, the binomial distribution one sample Kolmogorov Smirnov (KS) test was applied to determine whether average RIs or SIs were significantly above chance (above 50%). For analysis of N1 amplitude, Wilcoxon rank-sum test was used. Statistical tests on the electrophysiological time-frequency data were performed using the permutation method with <1,000 iterations [25] (see Supplementary Methods for full details). For all comparisons, alpha value was set at $p<0.05$.

RESULTS

Impaired sensory-motor gating in *Ehmt1*$^{D6Cre/+}$ mouse

The acoustic startle response and pre-pulse inhibition (PPI) of this response, were used to examine sensory-motor function in the *Ehmt1*$^{D6Cre/+}$ mice. Over the course of six consecutive auditory pulse (120dB) startle trials, *Ehmt1*$^{D6Cre/+}$ mice had, on average, twice the startle response compared to *Ehmt1*$^{fl/+}$ mice (Figure 1A; ANOVA, main effect of GENOTYPE, $F_{1,53}=6.86$, $p=0.01$). A significant interaction between GENOTYPE and TRIAL ($F_{3.87,201.0}=2.48$, $p=0.03$) indicated different patterns of startle reactivity and habituation relative to *Ehmt1*$^{fl/+}$ mice. *Post hoc* analysis revealed that there was an equivalent startle response to the initial trial between genotypes ($p=0.68$), but on average *Ehmt1*$^{D6Cre/+}$ mice showed a significantly enhanced startle response in all consecutive trials (trial 2, $p=0.05$; 3, $p=0.01$; 4, $p=0.001$; 5, $p=0.01$; and 6, $p=0.02$).

As expected, increasing the prepulse volume led to a linear increase in the inhibition of the startle in both groups (Figure 1B; ANOVA, main effect of PREPULSE, $F_{1.49,80.35}$=73.26, p=0.001). However, there was a 20-40% PPI reduction in the *Ehmt1*$^{D6Cre/+}$ mice relative to *Ehmt1*$^{fl/+}$ cage-mates (Figure 1B; ANOVA main effect of GENOTYPE, $F_{1,54}$=5.54, p=0.022), suggesting that, in addition to an enhanced startle response, the mutant mice were also impaired in the normal PPI response

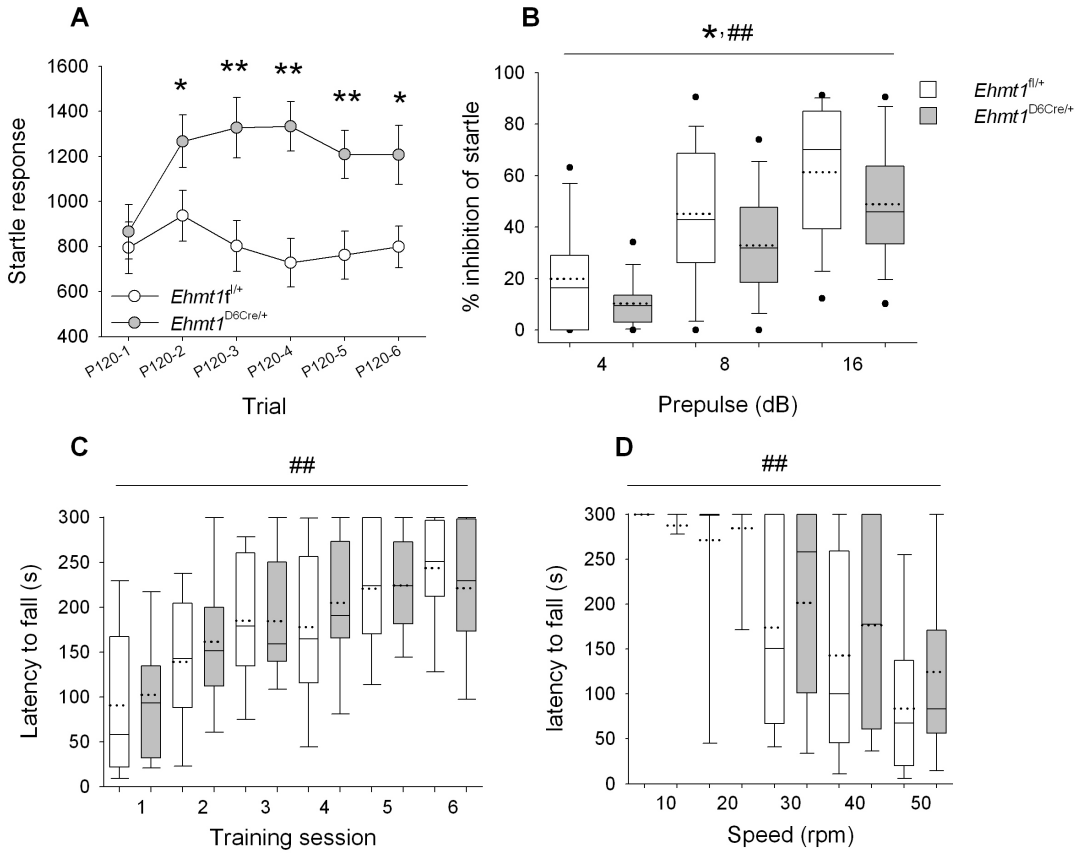

Figure 1. Sensory-motor gating & motor learning and coordination. A) The startle response after 6 consecutive 120dB pulse stimulations show *Ehmt1*$^{D6Cre/+}$ mice had a significantly higher overall maximum startle response in all trials. **B**) Prepulse inhibition of the startle response generally increased with the increasing volume of the prepulse as expected. However, *Ehmt1*$^{D6Cre/+}$ displayed a 20-40% reduction in PPI of startle relative to *Ehmt1*$^{fl/+}$ mice **C)** All animals improved motor ability on the rotarod as evidenced by an increase in latency to fall across 6 training sessions. There was no also difference in genotype during training **D)** In a probe test where rotarod speed accelerated throughout the session, there was a general decrease in the latency to fall as the speed increased, but again no difference between genotypes. Data are mean ±SEM, or box-plots showing median (solid line), mean (dotted line) and 10th, 25th and 75th and 90th percentiles. * represents main effect of GENOTYPE p<0.05; ## represents main effect of within-subject factor (TRIAL, PREPULSE, SESSION or SPEED).

Normal motor function in the *Ehmt1*$^{D6Cre/+}$ mouse

Altered sensory-motor gating in *Ehmt1*$^{D6Cre/+}$ mice was not due to any gross deficits in motoric competence. Training on the rotarod test indicated normal learning with repeated sessions, with latency to fall reducing across training sessions (Figure 1C; ANOVA, main effect of SESSION, $F_{5,130}$=21.33, p<0.001), but there was no difference in GENOTYPE ($F_{1,26}$=0.12, p=0.73) and no interaction between training SESSION and GENOTYPE ($F_{5,130}$=0.67, p=0.65). Moreover, in an accelerating rotarod probe test of motor coordination, latency to fall decreased as the speed increased (Figure 1D; ANOVA, main effect of SPEED, $F_{4,104}$=38.38, p<0.001), but there was no difference between GENOTYPE ($F_{1, 26}$=0.67, p=0.42) or interaction between SPEED and GENOTYPE ($F_{4,104}$=0.65, p =0.63).

Impaired novel object recognition in *Ehmt1*$^{D6Cre/+}$ mouse

The novel object recognition (NOR) task takes advantage of the preference of rodents to attend to new objects in their environment as a means for testing declarative memory [26]. Here, two inter-trial intervals were used: half of the cohort was examined following a 15-minute delay between the initial object exposure and the test trial, and half the cohort was examined after a 90-minute delay. In the test phase, as expected the *Ehmt1*$^{fl/+}$ control mice explored the novel object significantly more than chance (50%) in both the 15-minute and 90-minute retention trials (Figure 2A; Kolmogorov Smirnov test (KS), 15min, 60%, p=0. 02; 90min retention trial, 67%, p=0.002). However, exploration of the novel object by *Ehmt1*$^{D6Cre/+}$ mice was not significantly above chance, at either 15min (52%, $p=0.97$), or 90 min retention trial (50%, p=0.44).

This difference at test was not due to differences during the habituation phase, as indicated by overall exploration time of the object that was replaced by a novel object at test (*Ehmt1*$^{fl/+}$ mean=114s, ±SEM=15; *Ehmt1*$^{D6Cre/+}$ mean=113s ±SEM=12; ANOVA, no main effect of GENOTYPE, $F_{1,28}$=0.031, p=0.86).

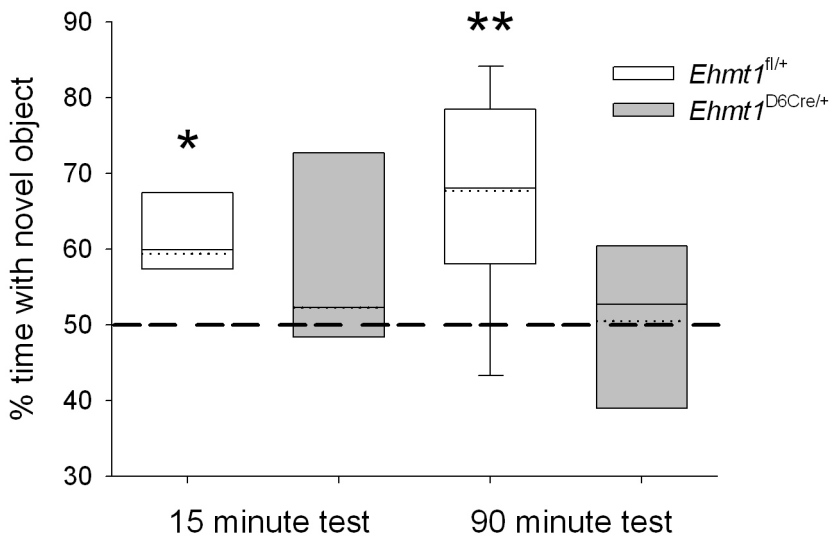

Figure 2. Novel object recognition. In both the 15-minute and 90-minute retention tests of the NOR task *Ehmt1*$^{fl/+}$ control mice explored the novel object more than chance. However, exploration of the novel object by *Ehmt1*$^{D6Cre/+}$ mice was not significantly above chance, for either the 15- or 90-minute retention trials indicating a deficit in declarative memory. Data are mean ±SEM or box-plots showing median (solid line), mean (dotted line) and 10th, 25th and 75th and 90th percentiles (dots represent 5th and 95th percentile). * represents main effect of GENOTYPE $p<0.05$; ** $p<0.01$.

Electrophysiological measurements of paired pulse AEPs

In order to gain an insight into the neural changes underpinning the deficits in sensory-motor gating seen in *Ehmt1*$^{D6Cre/+}$ mice we used electrophysiological methods. A subset of the behavioural cohort was then subject to EEG recording to measure auditory evoked potentials (AEPs). AEPs are voltage fluctuations time-locked to an auditory event used for brain dysfunction clinical diagnosis [27]. We used a paired pulse paradigm in which two pulses were delivered back-to-back with a 500ms interval between the first stimulus (S1) and the second stimulus (S2) (Figure 3A). The grand average waveforms show a stereotypic maximal positive deflection (P1) and maximal negative deflection (N1) (Figure 3B1). *Ehmt1*$^{D6Cre/+}$ mice had a nearly two-fold lower N1 amplitude response after the S1 (Figure 3B1) but not after S2 (Figure 3B2). Additionally, *Ehmt1*$^{D6Cre/+}$ mice had a significant reduction in the S2/S1 ratio for the N1 component (Wilcoxon, rank sum=64, p=0.018), what is considered an electrophysiological measurement of sensory gating (Figure 3C). During peak activation of the paired pulse

experiment we observed an increase in total power across high frequency bands from 10-100Hz in both groups of mice (Figure 3D1 and D2). The difference time-frequency plot and the permutation test between *Ehmt1*$^{D6Cre/+}$ and *Ehmt1*$^{fl/+}$ control mice however, revealed that the distributed peak that occurred approximately 40ms after the S1 pulse, a time corresponding with the N1, was significantly greater in the beta (13-30Hz) and gamma (30-70Hz) frequency bands in the *Ehmt1*$^{fl/+}$ control mice (Figure 3G1 and G2). The late (>200ms after the S1 pulse) decrease in the delta frequency band (~4Hz) prominent in *Ehmt1*$^{fl/+}$ (Figure 3D1-G1) was not different from *Ehmt1*$^{D6Cre/+}$ (Figure 3G2).

Measurements of evoked power, EEG power which is phase-locked with the event onset across trials, demonstrated increases in the delta (~4hz), beta (13-30Hz) and low gamma (here ~40Hz) band responses in both groups of mice approximately ~30-50 ms after the S1 (Figure 3E1 and E2). Again, permutation tests revealed a reduction in evoked power in *Ehmt1*$^{D6Cre/+}$ mice after both the S1 and ~40ms after the S2 pulse (Figure 3H1 and H2). In complement, we measured the phase locking factor (PLF), which provide a measurement of trial-to-trial reliability across the frequency domain [28]. To extract the PLF, magnitude information is transformed to 1 and averaged so that the phase angle with respect to event onset is extracted [29]. Values between zero and one are obtained, in which one reflects perfect synchrony of phase angles across trials. *Ehmt1*$^{D6Cre/+}$ mice did not show PLF values above .17 at any point, while control mice show nearly two-fold PLF synchrony (+.25) at ~40ms post-S1 pulse, between ~20-40Hz. Overall *Ehmt1*$^{D6Cre/+}$mice demonstrated reduced PLF (Figure 3F1 and F2).

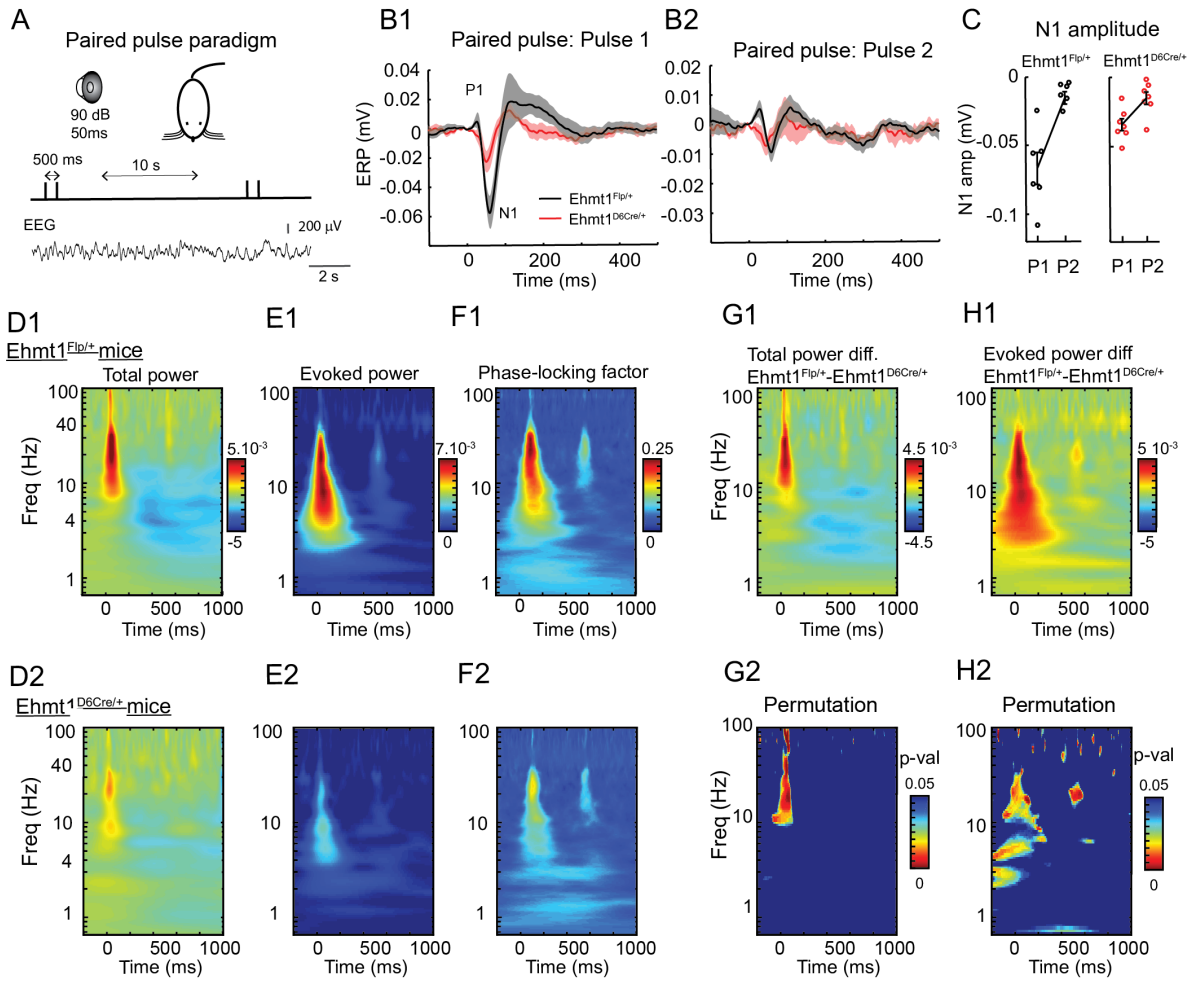

Figure 3. AEP paired pulse measurements

A) Schematic showing the paired pulse stimulus paradigm. **B1**) Grand average ERP waveform after pulse 1 (S1) in *Ehmt1*$^{D6Cre/+}$(red) *and Ehmt1*$^{fl/+}$ (black). The P1 and N1 components are indicated on the waveform. **B2**) The waveforms for pulse 2 (S2); **C)** N1 amplitude for *Ehmt1*$^{D6Cre/+}$ and *Ehmt1*$^{fl/+}$ mice. **D1 & D2)** Normalized total power (in time-frequency plot) of both S1 (time 0) and S2 (time 500ms) for *Ehmt1*$^{fl/+}$ (D1) and *Ehmt1*$^{D6Cre/+}$ (D2). Note the early increase in the beta/gamma range (10-100Hz) and the late decrease in the delta range (~4Hz) and the reduction of both components in the *Ehmt1*$^{D6Cre/+}$. **E1 & E2)** Evoked power time-frequency plots for the same data set; **F1 & F2)** Phase locking factor for the same data set; **G1)** Difference of total power between *Ehmt1*$^{fl/+}$ and *Ehmt1*$^{D6Cre/+}$. **G2)** Statistical significance heat map based on permutation tests of total power are indicated by the colour scale (p-value < 0.05); **H1)** Difference of evoked power between *Ehmt1*$^{fl/+}$ and *Ehmt1*$^{D6Cre/+}$ mice; **H2)** Statistical significance between evoked power of *Ehmt1*$^{fl/+}$ and *Ehmt1*$^{D6Cre/+}$ mice (spurious spots above 50Hz are due to occasional 50Hz noise contamination in some of the recordings). Data shown is mean ±SEM.

Electrophysiological measurements of Mismatched Negativity AEPs

The Mismatch Negativity (MMN) response is elicited when a qualitative feature of the stimulus does not match the pattern in a previous series [30] (Figure 4A). One core feature of MMN is the importance of NMDA receptor function. For instance, non-competitive NMDA antagonists, like ketamine and the selective antagonist of the NR2B NMDA subunit, CP-101,606 reduce MMN amplitude [31], the level of which predicts the magnitude of psychotic experiences in response to these drugs [32]. Therefore, in order to probe this function further here, mice were given either saline or 10mg/kg of ketamine prior to the MMN test.

In saline treated animals there was a difference between *Ehmt1*$^{D6Cre/+}$ and *Ehmt1*$^{fl/+}$ mice in response to the deviant pulse (Figures 4C-D) as indicated by analysis of the N1 amplitude that showed an interaction between GENOTYPE and PULSE (repeated measures ANOVA, $F_{1,8}$=12.70, p=0.007). In the standard pulse condition *Ehmt1*$^{fl/+}$ mice, amplitude corresponded to an increase in ~10-40Hz evoked potential approximately 30-50ms post-stimulus (Figure. 4C1-C2). In the deviant pulse condition, *Ehmt1*$^{fl/+}$ mice not only show an increase in ~10-40Hz evoked potential, but also one with greater peak latency, at 40-70ms post-stimulus (Figure 4C2). In contrast, *Ehmt1*$^{D6Cre/+}$ mice treated with saline showed no pattern of change in the amplitude response for either standard or deviant pulses.

However, following ketamine administration, the difference in the N1 amplitude between the standard and deviant pulse was absent for both genotypes (Figure 4B and D), as indicated by a lack of interaction between GENOTYPE and PULSE (repeated measures ANOVA, $F_{1,7}$=0.011, p=0.921). Further analysis underlined this finding. Permutation tests after saline administration for the deviant-only condition demonstrates a difference between *Ehmt1*$^{fl/+}$ controls and *Ehmt1*$^{D6Cre/+}$ wavelet transforms, at 30Hz between 50-80ms post-stimulus (Figure 4E1), driven by the higher amplitude response in the *Ehmt1*$^{fl/+}$ control mice. In contrast, after ketamine administration the difference in deviant response between *Ehmt1*$^{fl/+}$ controls and *Ehmt1*$^{D6Cre/+}$ mice was abolished (Figure 4E2).

Altered NMDA-receptor expression in *Ehmt1*$^{D6cre/+}$ mutant mice

In light of similarity in basal *Ehmt1*$^{D6Cre/+}$ electrophysiological phenotype and the electrophysiological phenotype in *Ehmt1*$^{fl/+}$ control mice following ketamine administration, we assessed the NMDA system in *Ehmt1*$^{D6Cre/+}$ mice. RT qPCR was used to examine the mRNA

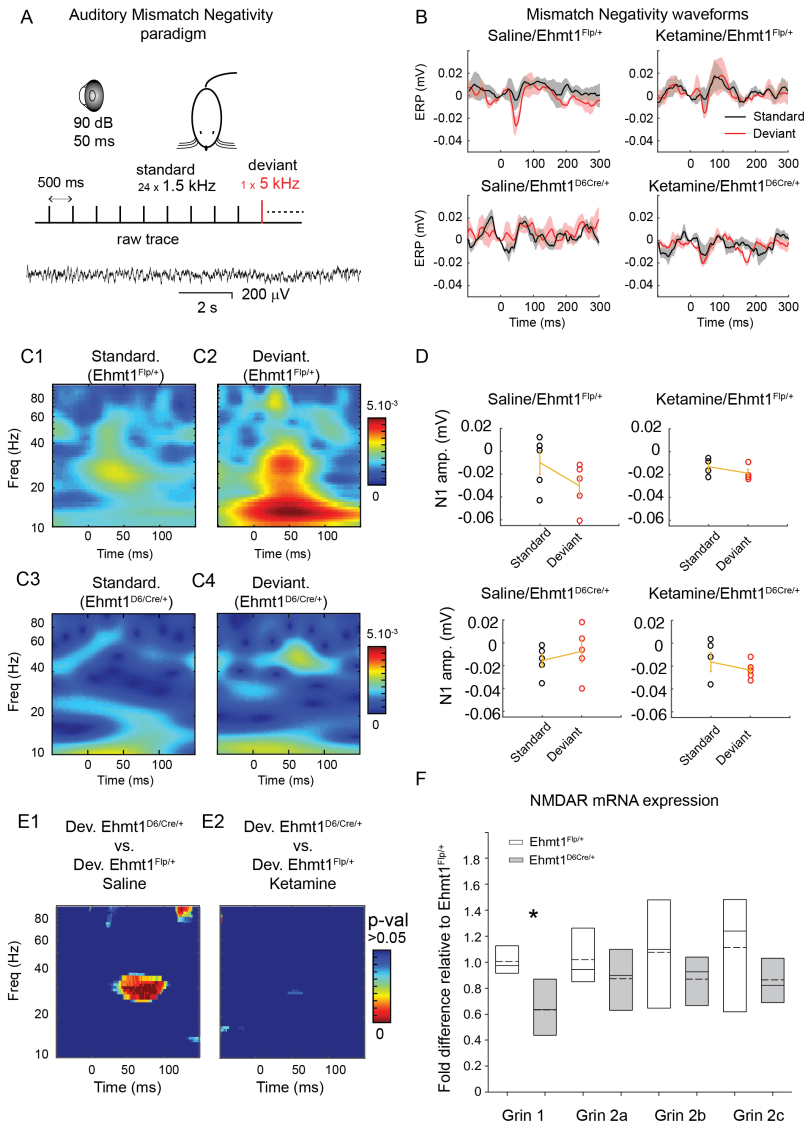

Figure 4. AEP mismatch negativity phenotypes & NMDA mRNA expression. A) Mismatch negativity stimulus **B)** Grand average ERP waveforms (shaded areas) after the saline or ketamine conditions in the in *Ehmt1*$^{fl/+}$ and *Ehmt1*$^{D6Cre/+}$, for the deviant (red) and standard (black) tone for each condition. **C1 & C2)** Time-frequency plot of evoked power for the standard and deviant pulse in *Ehmt1*$^{fl/+}$ mice after saline injection; **C3 & C4)** Time-frequency plot of evoked power for the standard and deviant pulse in *Ehmt1*$^{D6Cre/+}$mice following saline injection. **D)** N1 amplitude peak amplitude corresponding to each condition. **E1)** Permutation test showing heat map of *p*-values for the difference of distribution between deviant tone maps of saline treated *Ehmt1*$^{fl/+}$ (C2) and *Ehmt1*$^{D6Cre/+}$ (C4). **E2)** Permutation test showing heat map of *p*-values for the difference of distribution between deviant tone maps of ketamine treated *Ehmt1*$^{fl/+}$ (C2) and *Ehmt1*$^{D6Cre/+}$ (C4). **F)** NMDA subunit mRNA expression in hippocampal samples. Data shown is mean ±SEM or box-plots showing median (solid line), mean (dashed line) and 10th, 25th and 75th and 90th percentiles. * represents main effect of GENOTYPE $p<0.05$.

levels of NMDA-R subunits *Grin1*, *Grin2a*, *Grin2b* and *Grin2c* in the adult hippocampus. Expression of *Grin1*, the gene encoding NMDA NR1 subunit, was significantly reduced by 40% on average in *Ehmt1*$^{D6cre/+}$ mice (Figure 4F; t=3.50, *p*=0.006). No difference was seen in *Grin2a* (t=0.99, *p*=0.342), *Grin2b* (t=0.87, *p*=0.434), or *Grin2c* (t=-1.02, *p*=0.498) expression.

DISCUSSION

Recent studies in human genomics strongly implicate a number of genes found to regulate chromatin dynamics in the etiology of neurodevelopmental disorders from developmental delays [6], to autism spectrum disorders [3, 4], and schizophrenia [5]. *EHMT1* is one such gene, associated with both neurodevelopmental and neuropsychiatric disorders. Here we examined behavioural and electrophysiological correlates of information processing in a mouse model of *Ehmt1* haploinsufficiency, specifically in the forebrain. We found that *Ehmt1*$^{D6Cre/+}$ mice have sensorimotor and auditory gating deficits, and learning and memory deficits, in the absence of generic deficits in motor function. *Ehmt1*$^{D6Cre/+}$ mice also showed a number of abnormalities in electrophysiological measurements including a reduced magnitude of AEPs after paired-pulse inhibition and MMN tasks, reduced evoked and total power in high frequency bands, and reduce PLF. Overall these data indicate that *Ehmt1*$^{D6Cre/+}$ mice show deficits in sensory motor gating and information process, possibly related to abnormal NMDA functioning.

EHMT1 is a risk gene associated with a number of neurodevelopmental and psychiatric disorders [8], thus it was important for this work to focus not only on translational phenotypes but those that overlap traditional diagnostic boundaries. Several prominent features shared by these disorders are associated with deficits in attention and gating, or filtering out intrusive stimuli [33-36]. Behaviorally, the *Ehmt1*$^{D6Cre/+}$ mice showed evidence of this in an acoustic startle test. Sensory motor gating deficits were manifest by both a greatly enhanced acoustic startle response, and a decreased pre-pulse inhibition of startle. We explored this further by examining electrophysiological measures of gating. *Ehmt1*$^{D6Cre/+}$ had reduced N1 amplitude in response to stimulus 1 (S1). Furthermore, *Ehmt1*$^{D6Cre/+}$ mice had a significant reduction in the S2/S1 ratio for the N1 component, an electrophysiological correlate of sensory gating.

Information-processing deficits are another common phenotype associated with *EHMT1* risk populations. Accordingly, *Ehmt1*$^{D6Cre/+}$ mice were examined on their performance in the NOR

task, a paradigm where an animal's ability to remember a previously encountered object is indicated by an increased willingness to explore the novel object over the familiar object. The *Ehmt1*$^{D6Cre/+}$ mice showed no evidence of novel object recognition, even with only a 15-minute interval after habituation. Importantly, this was not due to reduced interest in exploration or exposure to the familiar object, as time spent in exploration was equivalent across *Ehmt1*$^{fl/+}$ control and *Ehmt1*$^{D6Cre/+}$ mutant mice.

Further, electrophysiological evidence of information-processing deficits in the *Ehmt1*$^{D6Cre/+}$ mice was provided by the reduced response in a mismatch negativity (MMN) paradigm. The decreased amplitude responses in these AEP measurements meanwhile corresponded to significant reductions in total and evoked power in high frequency bands. Such reductions may be particularly insightful, as numerous studies report disruptions in gamma-band activity across neurodevelopment [34, 37], neuropsychiatric [38] and neurodegenerative diseases [39]. Whether reduced gamma activity is actually directly associated with disease pathologies across these patient populations remains largely unknown. Recently however, reductions in gamma-band activity were found to precede the onset of plaque formations and cognitive decline in a mouse model of Alzheimer's disease. Meanwhile the stimulation of fast-spiking interneurons in the gamma frequency range (~40Hz), a way to boost gamma-band activity [40], led to the reduction in the plaque forming amyloid isoforms and attenuated plaque load in ageing mice [39]. In a more functional assessment, the induction of long-term potentiation using high frequency stimulation (~100Hz) was found to restore spine density and long-term memory in early stages of the disease in mice [41]. While these findings are specific to Alzheimer's disease, they also confirm an important link between gamma synchrony and cognitive function exists [42]. Furthermore, we may find disruptions in high frequency oscillation patterns tightly correspond with the degree of cognitive impairment and range of pathologies across *EHMT1* risk populations.

The decreases in high frequency activity coupled with reduced *Grin1* mRNA are suggestive of overall disruptions in local connectivity and may hint to more global imbalances in excitation/inhibition (E/I). Such findings do corroborate previous reports showing changes in *Ehmt1*-mediated H3K9me2 levels dynamically regulate synaptic scaling, thus playing a direct role in the fine balance between excitation and inhibition at the level of individual neurons [17]. And indeed many of the *Ehmt1*$^{D6Cre/+}$ mice phenotypes are markedly similar to *Grin1* mouse

mutants [43]. The *Grin1*$^{neo-/-}$ mice and the *Grin1*^{Rgsc174} heterozygous mice both show novelty induced hyperactivity, increased stereotypy [44] and deficits in sensorimotor gating [45]. Mice with even subtle reductions in the NR1 receptor are found to have decreases in MMN [46], gamma-band disruptions and reduction in E/I balance [47]. Thus future investigation of the *Ehmt1* haploinsufficiency may benefit from further examination of the relationship between reductions in gamma-band activity and NMDA-hypofunction.

In summary, *Ehmt1*$^{D6Cre/+}$ forebrain-specific haploinsufficiency produced deficits in sensory-gating and information processing. Behavioural evidence from explicit tests of sensorimotor gating and findings from a learning and memory task, suggest that *Ehmt1*$^{D6Cre/+}$ mice do not attend to or process information in order to inform appropriate behavioural responses. Neural correlates of these abnormalities were further demonstrated using electrophysiological studies, which indicated deficits related to disruptions in local connectivity and NMDA function. Taken together these data suggest that *Ehmt1* haploinsufficiency leads to abnormal circuit formation and behavioural abnormalities that likely underpin deficits seen across the broad spectrum of neurodevelopmental and neuropsychiatric disorders with which *EHMT1* is associated.

Conflict of interest statement

The authors have no interests in any company or organization that would benefit from this article.

Funding

This work was funded by a Wellcome Trust Integrative Neuroscience PhD grant (WT093765MA) to BAD, AJH and ARI. VC was supported by a Wellcome Trust Programme Grant (91882). ARI and AJH are members of the MRC Centre for Neuropsychiatric Genetics and Genomics (G0801418).

REFERENCES

1. Tyssowski K, Kishi Y, Gotoh Y. Chromatin regulators of neural development. Neuroscience. 2014;264:4-16. doi: 10.1016/j.neuroscience.2013.10.008. PubMed PMID: 24144622.
2. Hirabayashi Y, Gotoh Y. Epigenetic control of neural precursor cell fate during development. Nature reviews Neuroscience. 2010;11(6):377-88. doi: 10.1038/nrn2810. PubMed PMID: 20485363.
3. RK CY, Merico D, Bookman M, J LH, Thiruvahindrapuram B, Patel RV, et al. Whole genome sequencing resource identifies 18 new candidate genes for autism spectrum disorder. Nature neuroscience. 2017. doi: 10.1038/nn.4524. PubMed PMID: 28263302.
4. De Rubeis S, He X, Goldberg AP, Poultney CS, Samocha K, Cicek AE, et al. Synaptic, transcriptional and chromatin genes disrupted in autism. Nature. 2014;515(7526):209-15. doi: 10.1038/nature13772. PubMed PMID: 25363760; PubMed Central PMCID: PMCPMC4402723.
5. Network, Pathway Analysis Subgroup of Psychiatric Genomics C. Psychiatric genome-wide association study analyses implicate neuronal, immune and histone pathways. Nature neuroscience. 2015;18(2):199-209. doi: 10.1038/nn.3922. PubMed PMID: 25599223; PubMed Central PMCID: PMCPMC4378867.
6. Singh T, Kurki MI, Curtis D, Purcell SM, Crooks L, McRae J, et al. Rare loss-of-function variants in SETD1A are associated with schizophrenia and developmental disorders. Nature neuroscience. 2016;19(4):571-7. doi: 10.1038/nn.4267. PubMed PMID: 26974950.
7. Deciphering Developmental Disorders S. Prevalence and architecture of de novo mutations in developmental disorders. Nature. 2017. doi: 10.1038/nature21062. PubMed PMID: 28135719.
8. Talkowski ME, Rosenfeld JA, Blumenthal I, Pillalamarri V, Chiang C, Heilbut A, et al. Sequencing chromosomal abnormalities reveals neurodevelopmental loci that confer risk across diagnostic boundaries. Cell. 2012;149(3):525-37. doi: 10.1016/j.cell.2012.03.028. PubMed PMID: 22521361; PubMed Central PMCID: PMC3340505.
9. Kleefstra T, Brunner HG, Amiel J, Oudakker AR, Nillesen WM, Magee A, et al. Loss-of-function mutations in euchromatin histone methyl transferase 1 (EHMT1) cause the 9q34 subtelomeric deletion syndrome. American journal of human genetics. 2006;79(2):370-7. doi: 10.1086/505693. PubMed PMID: 16826528; PubMed Central PMCID: PMC1559478.
10. Kleefstra T, Smidt M, Banning MJ, Oudakker AR, Van Esch H, de Brouwer AP, et al. Disruption of the gene Euchromatin Histone Methyl Transferase1 (Eu-HMTase1) is associated with the 9q34 subtelomeric deletion syndrome. J Med Genet. 2005;42(4):299-306. doi: 10.1136/jmg.2004.028464. PubMed PMID: 15805155; PubMed Central PMCID: PMCPMC1736026.
11. Cooper GM, Coe BP, Girirajan S, Rosenfeld JA, Vu TH, Baker C, et al. A copy number variation morbidity map of developmental delay. Nature genetics. 2011;43(9):838-46. Epub 2011/08/16. doi: 10.1038/ng.909. PubMed PMID: 21841781; PubMed Central PMCID: PMC3171215.
12. O'Roak BJ, Vives L, Girirajan S, Karakoc E, Krumm N, Coe BP, et al. Sporadic autism exomes reveal a highly interconnected protein network of de novo mutations. Nature. 2012;485(7397):246-50. Epub 2012/04/13. doi: 10.1038/nature10989. PubMed PMID: 22495309; PubMed Central PMCID: PMC3350576.

13. Kirov G, Pocklington AJ, Holmans P, Ivanov D, Ikeda M, Ruderfer D, et al. De novo CNV analysis implicates specific abnormalities of postsynaptic signalling complexes in the pathogenesis of schizophrenia. Molecular psychiatry. 2012;17(2):142-53. Epub 2011/11/16. doi: 10.1038/mp.2011.154. PubMed PMID: 22083728; PubMed Central PMCID: PMC3603134.
14. Balemans MC, Huibers MM, Eikelenboom NW, Kuipers AJ, van Summeren RC, Pijpers MM, et al. Reduced exploration, increased anxiety, and altered social behavior: Autistic-like features of euchromatin histone methyltransferase 1 heterozygous knockout mice. Behavioural brain research. 2010;208(1):47-55. Epub 2009/11/10. doi: 10.1016/j.bbr.2009.11.008. PubMed PMID: 19896504.
15. Gupta-Agarwal S, Franklin AV, Deramus T, Wheelock M, Davis RL, McMahon LL, et al. G9a/GLP histone lysine dimethyltransferase complex activity in the hippocampus and the entorhinal cortex is required for gene activation and silencing during memory consolidation. The Journal of neuroscience : the official journal of the Society for Neuroscience. 2012;32(16):5440-53. doi: 10.1523/JNEUROSCI.0147-12.2012. PubMed PMID: 22514307; PubMed Central PMCID: PMCPMC3332335.
16. Gupta NA, Mells J, Dunham RM, Grakoui A, Handy J, Saxena NK, et al. Glucagon-like peptide-1 receptor is present on human hepatocytes and has a direct role in decreasing hepatic steatosis in vitro by modulating elements of the insulin signaling pathway. Hepatology. 2010;51(5):1584-92. doi: 10.1002/hep.23569. PubMed PMID: 20225248; PubMed Central PMCID: PMCPMC2862093.
17. Benevento M, Iacono G, Selten M, Ba W, Oudakker A, Frega M, et al. Histone Methylation by the Kleefstra Syndrome Protein EHMT1 Mediates Homeostatic Synaptic Scaling. Neuron. 2016;91(2):341-55. doi: 10.1016/j.neuron.2016.06.003. PubMed PMID: 27373831.
18. Schaefer A, Sampath SC, Intrator A, Min A, Gertler TS, Surmeier DJ, et al. Control of cognition and adaptive behavior by the GLP/G9a epigenetic suppressor complex. Neuron. 2009;64(5):678-91. doi: 10.1016/j.neuron.2009.11.019. PubMed PMID: 20005824; PubMed Central PMCID: PMCPMC2814156.
19. McNamara GI, Davis BA, Dwyer DM, John RM, Isles AR. Behavioural abnormalities in a novel mouse model for Silver Russell Syndrome. Human molecular genetics. 2016;25(24):5407-17. doi: 10.1093/hmg/ddw357. PubMed PMID: 27798108.
20. Ehrlichman RS, Maxwell CR, Majumdar S, Siegel SJ. Deviance-elicited changes in event-related potentials are attenuated by ketamine in mice. J Cogn Neurosci. 2008;20(8):1403-14. doi: 10.1162/jocn.2008.20097. PubMed PMID: 18303985.
21. Siegel SJ, Connolly P, Liang Y, Lenox RH, Gur RE, Bilker WB, et al. Effects of strain, novelty, and NMDA blockade on auditory-evoked potentials in mice. Neuropsychopharmacology : official publication of the American College of Neuropsychopharmacology. 2003;28(4):675-82. doi: 10.1038/sj.npp.1300087. PubMed PMID: 12655312.
22. Kronland-Martinet R, Morlet J, Grossmann A. Analysis of sound patterns through wavelet transforms. International journal of pattern recognition and artificial intelligence. 1987;1(02):273-302. doi: 10.1142/S0218001487000205.
23. Halene TB, Ehrlichman RS, Liang Y, Christian EP, Jonak GJ, Gur TL, et al. Assessment of NMDA receptor NR1 subunit hypofunction in mice as a model for schizophrenia. Genes, brain, and behavior. 2009;8(7):661-75. doi: 10.1111/j.1601-183X.2009.00504.x. PubMed PMID: 19563516; PubMed Central PMCID: PMCPMC2757454.

24. Livak KJ, Schmittgen TD. Analysis of relative gene expression data using real-time quantitative PCR and the 2(-Delta Delta C(T)) Method. Methods. 2001;25(4):402-8. PubMed PMID: 11846609.
25. Westfall PH, Young SS. Resampling-based multiple testing: Examples and methods for p-vlaue adjustment. New York: Wiley; 1993.
26. Antunes M, Biala G. The novel object recognition memory: neurobiology, test procedure, and its modifications. Cogn Process. 2012;13(2):93-110. doi: 10.1007/s10339-011-0430-z. PubMed PMID: 22160349; PubMed Central PMCID: PMCPMC3332351.
27. Luck SJ, Mathalon DH, O'Donnell BF, Hamalainen MS, Spencer KM, Javitt DC, et al. A roadmap for the development and validation of event-related potential biomarkers in schizophrenia research. Biological psychiatry. 2011;70(1):28-34. doi: 10.1016/j.biopsych.2010.09.021. PubMed PMID: 21111401; PubMed Central PMCID: PMCPMC3116072.
28. Goffin D, Brodkin ES, Blendy JA, Siegel SJ, Zhou Z. Cellular origins of auditory event-related potential deficits in Rett syndrome. Nature neuroscience. 2014;17(6):804-6. doi: 10.1038/nn.3710. PubMed PMID: 24777420; PubMed Central PMCID: PMCPMC4038660.
29. Roach BJ, Mathalon DH. Event-related EEG time-frequency analysis: an overview of measures and an analysis of early gamma band phase locking in schizophrenia. Schizophrenia bulletin. 2008;34(5):907-26. doi: 10.1093/schbul/sbn093. PubMed PMID: 18684772; PubMed Central PMCID: PMCPMC2632478.
30. Light GA, Braff DL. Stability of mismatch negativity deficits and their relationship to functional impairments in chronic schizophrenia. The American journal of psychiatry. 2005;162(9):1741-3. doi: 10.1176/appi.ajp.162.9.1741. PubMed PMID: 16135637.
31. Sivarao DV, Chen P, Yang Y, Li YW, Pieschl R, Ahlijanian MK. NR2B Antagonist CP-101,606 Abolishes Pitch-Mediated Deviance Detection in Awake Rats. Front Psychiatry. 2014;5:96. doi: 10.3389/fpsyt.2014.00096. PubMed PMID: 25140157; PubMed Central PMCID: PMCPMC4122188.
32. Umbricht D, Koller R, Vollenweider FX, Schmid L. Mismatch negativity predicts psychotic experiences induced by NMDA receptor antagonist in healthy volunteers. Biological psychiatry. 2002;51(5):400-6. PubMed PMID: 11904134.
33. Javitt DC. Sensory processing in schizophrenia: neither simple nor intact. Schizophrenia bulletin. 2009;35(6):1059-64. doi: 10.1093/schbul/sbp110. PubMed PMID: 19833806; PubMed Central PMCID: PMCPMC2762632.
34. Orekhova EV, Stroganova TA, Prokofyev AO, Nygren G, Gillberg C, Elam M. Sensory gating in young children with autism: relation to age, IQ, and EEG gamma oscillations. Neuroscience letters. 2008;434(2):218-23. doi: 10.1016/j.neulet.2008.01.066. PubMed PMID: 18313850.
35. Perry W, Minassian A, Lopez B, Maron L, Lincoln A. Sensorimotor gating deficits in adults with autism. Biological psychiatry. 2007;61(4):482-6. doi: 10.1016/j.biopsych.2005.09.025. PubMed PMID: 16460695.
36. Belmonte MK, Cook EH, Jr., Anderson GM, Rubenstein JL, Greenough WT, Beckel-Mitchener A, et al. Autism as a disorder of neural information processing: directions for research and targets for therapy. Molecular psychiatry. 2004;9(7):646-63. doi: 10.1038/sj.mp.4001499. PubMed PMID: 15037868.
37. Kwon JS, O'Donnell BF, Wallenstein GV, Greene RW, Hirayasu Y, Nestor PG, et al. Gamma frequency-range abnormalities to auditory stimulation in schizophrenia. Archives of

general psychiatry. 1999;56(11):1001-5. PubMed PMID: 10565499; PubMed Central PMCID: PMCPMC2863027.
38. Tatard-Leitman VM, Jutzeler CR, Suh J, Saunders JA, Billingslea EN, Morita S, et al. Pyramidal cell selective ablation of N-methyl-D-aspartate receptor 1 causes increase in cellular and network excitability. Biological psychiatry. 2015;77(6):556-68. doi: 10.1016/j.biopsych.2014.06.026. PubMed PMID: 25156700; PubMed Central PMCID: PMCPMC4297754.
39. Iaccarino HF, Singer AC, Martorell AJ, Rudenko A, Gao F, Gillingham TZ, et al. Gamma frequency entrainment attenuates amyloid load and modifies microglia. Nature. 2016;540(7632):230-5. doi: 10.1038/nature20587. PubMed PMID: 27929004.
40. Cardin JA, Carlen M, Meletis K, Knoblich U, Zhang F, Deisseroth K, et al. Driving fast-spiking cells induces gamma rhythm and controls sensory responses. Nature. 2009;459(7247):663-7. doi: 10.1038/nature08002. PubMed PMID: 19396156; PubMed Central PMCID: PMCPMC3655711.
41. Roy DS, Arons A, Mitchell TI, Pignatelli M, Ryan TJ, Tonegawa S. Memory retrieval by activating engram cells in mouse models of early Alzheimer's disease. Nature. 2016;531(7595):508-12. doi: 10.1038/nature17172. PubMed PMID: 26982728; PubMed Central PMCID: PMCPMC4847731.
42. Fries P. Rhythms for Cognition: Communication through Coherence. Neuron. 2015;88(1):220-35. doi: 10.1016/j.neuron.2015.09.034. PubMed PMID: 26447583; PubMed Central PMCID: PMCPMC4605134.
43. Furuse T, Wada Y, Hattori K, Yamada I, Kushida T, Shibukawa Y, et al. Phenotypic characterization of a new Grin1 mutant mouse generated by ENU mutagenesis. The European journal of neuroscience. 2010;31(7):1281-91. doi: 10.1111/j.1460-9568.2010.07164.x. PubMed PMID: 20345915.
44. Mohn AR, Gainetdinov RR, Caron MG, Koller BH. Mice with reduced NMDA receptor expression display behaviors related to schizophrenia. Cell. 1999;98(4):427-36. PubMed PMID: 10481908.
45. Duncan GE, Moy SS, Perez A, Eddy DM, Zinzow WM, Lieberman JA, et al. Deficits in sensorimotor gating and tests of social behavior in a genetic model of reduced NMDA receptor function. Behavioural brain research. 2004;153(2):507-19. doi: 10.1016/j.bbr.2004.01.008. PubMed PMID: 15265649.
46. Featherstone RE, Shin R, Kogan JH, Liang Y, Matsumoto M, Siegel SJ. Mice with subtle reduction of NMDA NR1 receptor subunit expression have a selective decrease in mismatch negativity: Implications for schizophrenia prodromal population. Neurobiology of disease. 2015;73:289-95. doi: 10.1016/j.nbd.2014.10.010. PubMed PMID: 25461194.
47. Gandal MJ, Sisti J, Klook K, Ortinski PI, Leitman V, Liang Y, et al. GABAB-mediated rescue of altered excitatory-inhibitory balance, gamma synchrony and behavioral deficits following constitutive NMDAR-hypofunction. Transl Psychiatry. 2012;2:e142. doi: 10.1038/tp.2012.69. PubMed PMID: 22806213; PubMed Central PMCID: PMCPMC3410621.